Laser-based Sensing, Measurement and Misalignment Control of Coupled Linear and Angular Motion for Ultra-High Precision Movement

Leon Clark[1], Bijan Shirinzadeh[1], Yanling Tian[2], and Denny Oetomo[3]

Abstract

This paper presents a novel methodology for position and orientation (pose) measurement of stages used for micro/nano positioning which produce coupled motions with three planar degrees of freedom (DOF). In the proposed methodology, counter-rotation of the entire mechanism prevents the misalignment of the measurement beams within a laser-interferometry-based sensing and measurement technique. To detect such misalignment, a sensing strategy constructed around a position sensitive diode has been developed. A feedforward-feedback compound controller has been established to provide the necessary counter-rotation input to reduce misalignment error. Experimental validation has been conducted through measurement of the workspace of a three DOF planar micro/nano positioning stage. Experimental results demonstrate the capability of the technique to provide combined linear/angular measurement.

Keywords: micro/nano positioning, coupled 3DOF motion, laser interferometer based sensing

1 Introduction

Mechanisms for micro/nano positioning play a critical role in many technologies at the micro- and nanometer scale. Such mechanisms enable instrumentation such as Atomic Force Microscopes (AFMs), Scanning Tunneling Microscopes (STMs), Scanning Electron Microscopes (SEMs) and lithographic processes, and have potential applications in micro-manufacturing and assembly, microchip fabrication, optical steering, and many more [1–7]. The developments in this field, such as actuators with increased precision and faster response, higher resolution measurement techniques, and more advanced control methodologies, have improved the positioning performance of such mechanisms. In turn, all of these

[1] L. Clark and B. Shirinzadeh are with the Robotics and Mechatronics Research Laboratory, Department of Mechanical and Aerospace Engineering, Monash University, Clayton, VIC 3800, Australia (email: leon.clark@monash.edu, bijan.shirinzadeh@monash.edu)

[2] Y. Tian is with the Key Laboratory of Mechanism Theory and Equipment Design of Ministry of Education, Tianjin University, Tianjin 30072, China (email: meytian@tju.edu.cn)

[3] D. Oetomo is with the Department of Mechanical Engineering, Melbourne University, Melbourne VIC 3010, Australia (email: doetomo@unimelb.edu.au)

applications have benefited from such advancements, resulting in improved image resolution, lower manufacturing tolerances, and so on.

Conventional kinematic pairs such as revolute and prismatic joints exhibit friction and backlash which prohibit their use within the design of such positioners. Consequently, micro/nano positioning mechanisms typically employ compliant design techniques, which permit continuous, smooth motion free from these effects. Similarly, the use of piezoelectric actuators (PEAs) to provide input to the mechanism produces sub-nanometer actuation with infinite resolution whilst having high stiffness [8]. Combining these together has allowed the development of high precision positioners exhibiting fast response.

Research efforts have been directed towards the development of positioning stages which produce linear motion with up to three degrees of freedom [9–14]. Typically these have been designed from parallel kinematic chains; however stacked serial mechanisms have also been produced [15]. Due to non-linear effects including hysteresis and drift present within each PEA's response, the development of reliable control methodologies are mandated. Previous studies have proposed feedback and feedforward control methodologies to improve tracking performance [16–22]. For such feedback and verification purposes, capacitive and laser-based sensing and measurement techniques have commonly been employed to measure the displacement at the micro/nano scale.

Mechanisms with a greater number of degrees of freedom have also been developed, which are therefore capable of producing angular motion [23–27]. Resulting from the limitations presented by the wire electrical discharge machining (WEDM) process, the majority of these stages have three planar degrees of freedom, allowing motion in the X, Y and θ directions. For the design of such mechanisms, the three revolute-revolute-revolute (3-RRR) kinematic chain has gained favor. The angular range of these stages is dependent on the geometric properties of the mechanism, in particular the ratios of linkage lengths, as well as the capabilities of the actuators. Typically, this angular range is in the vicinity of 1–5 mrad.

Research focused towards angular motion has resulted in the development of numerous techniques for high resolution angular measurement. These include autocollimators, interferometers, Position Sensitive Diode (PSD) based methods and image based methods [28–33]. Many of these function through measurement of the arc length after the deflection of a laser beam. For these schemes, an increase in the resolution results in a loss of measurement range – which is often less than 0.5 mrad. However, some techniques have allowed this range to be extended, such as the use of retroreflectors to minimize beam misalignment [34].

Many of these measurement methods are unsuitable for use with mechanisms for micro/nano positioning. The requirement to produce linear motion coupled to rotation introduces geometric errors into sensor data, or worse can cause beam misalignment preventing correct sensor function. Due to these issues, little research effort has been devoted to the actuation, control and measurement of a mechanism's pose throughout its entire workspace. The three DOF systems of Yeh *et al.* [35] and Choi *et al.* [36], as well as the six DOF systems of Hrabina *et al.* [37] and Lazar *et al.* [38], used laser-interferometry-based measurement techniques to monitor all axes of motion. In all cases, any rotation was considered to be an error, which a controller would aim to minimize. The maximum
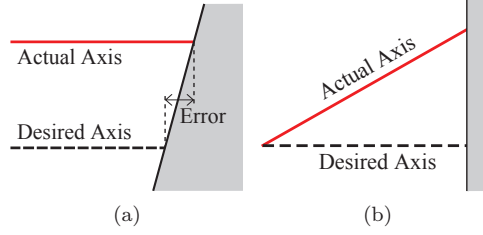
Figure 1: Geometric errors introduced by misalignment within measurement systems: (a) Abbe error, (b) Cosine error.

angular displacement under feedback control observed in any of these studies was 7 μrad.

In this paper, a methodology to enable pose measurement of a three DOF planar positioner is developed and experimentally verified. It is based upon a tracking process which counter-rotates the target reflector for a laser-based sensing and measurement technique, preventing the misalignment of the measurement beams. In order to detect such misalignment for closed-loop control, a PSD-based measurement methodology is developed. Furthermore, modeling of the system response is performed to produce a feedforward-feedback compound controller. Extensive experimentation is conducted to verify the performance of the system, and experimental results are presented.

2   Misalignment within Measurement Systems

In this paper, the attention is directed towards the use of laser-interferometry-based sensing and measurement techniques. This stems from their practically unlimited range with sub-nanometer resolution for linear displacement measurement and fast response, making these well suited for feedback control [39]. These systems, which typically employ homodyne or heterodyne interferometry techniques, require careful alignment of the laser beams which traverse the apparatus to produce the requisite interference pattern at the photodetector.

The introduction of tilt of the target mirror therefore produces two undesirable effects. The first of these is the misalignment of the beams within the system, which can either impede the performance of the interferometer, or worse cause misalignment to such an extent that the interference pattern can no longer be measured. The second effect is the introduction of geometric errors within the system output. These can take the form of Abbe and cosine errors, as illustrated in Fig. 1. Abbe errors will be introduced when the actual measurement axis does not coincide with the desired axis, but can be minimized through careful apparatus setup. Cosine errors, however, are inherent to the production of rotational motion. Thus, it is desirable to minimize such tilt to optimize the performance of laser-interferometry-based sensing and measurement methodologies.

This of course is contradictory to the objective of the measurement of coupled motions in both linear and rotational axes. To this end, this paper proposes a method to enable measurement of pose over a wide range, whilst simultaneously permitting the utilization of laser-interferometry-based sensing
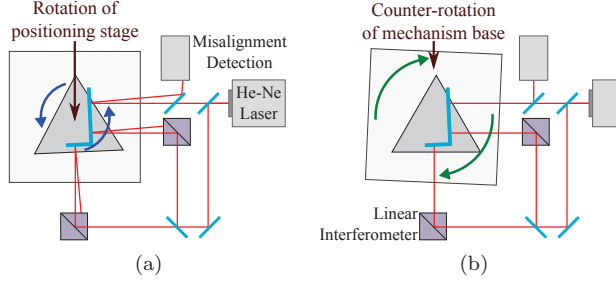
3

Figure 2: Schematic of proposed pose measurement methodology. (a) Rotational actuation of positioning stage induces misalignment in optical system. (b) Misalignment is compensated through counter-rotation of base.
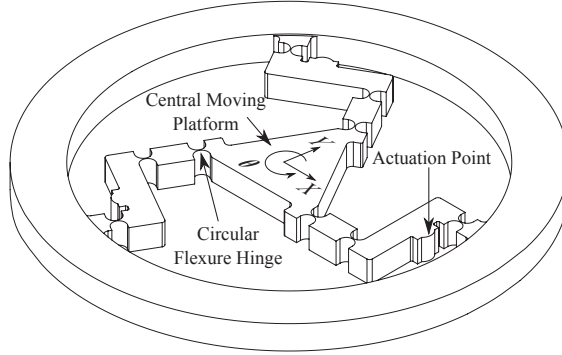

Figure 3: The 3-RRR compliant flexure-based mechanism utilized for experimentation.

and measurement techniques for displacements in the linear axes. This technique resembles tracking schemes which have been employed to measure the pose of end-effectors of robotic arms [40]. This methodology employs a steering assembly fixed beneath the base of the positioning mechanism to provide a counter-rotation to the stage's angular motion, thus preventing the laser system from exposure to beam misalignment. A schematic of the proposed methodology is provided in Fig. 2.

For this apparatus, two linear interferometer axes measure the motion of the platform in the X and Y directions. A misalignment detection strategy, which shares the same laser source, measures the deflection of the laser beam due to stage tilt. The output of this sensor provides an error signal to a controller which will rotate the entire mechanism-base assembly in the opposite direction to the misalignment. As the counter-rotation will exactly compensate for the rotation of the mechanism's stage, measurement of θ is performed by recording the counter-rotation.

3   Experimental Apparatus

A 3-RRR flexure-based mechanism, as shown in Fig. 3, has been utilized as an experimental platform to produce motion with three degrees of freedom [26]. The steering assembly which provides the counter-rotation consists of a precision rotation stage driven by a micro-stepping drive. The drive
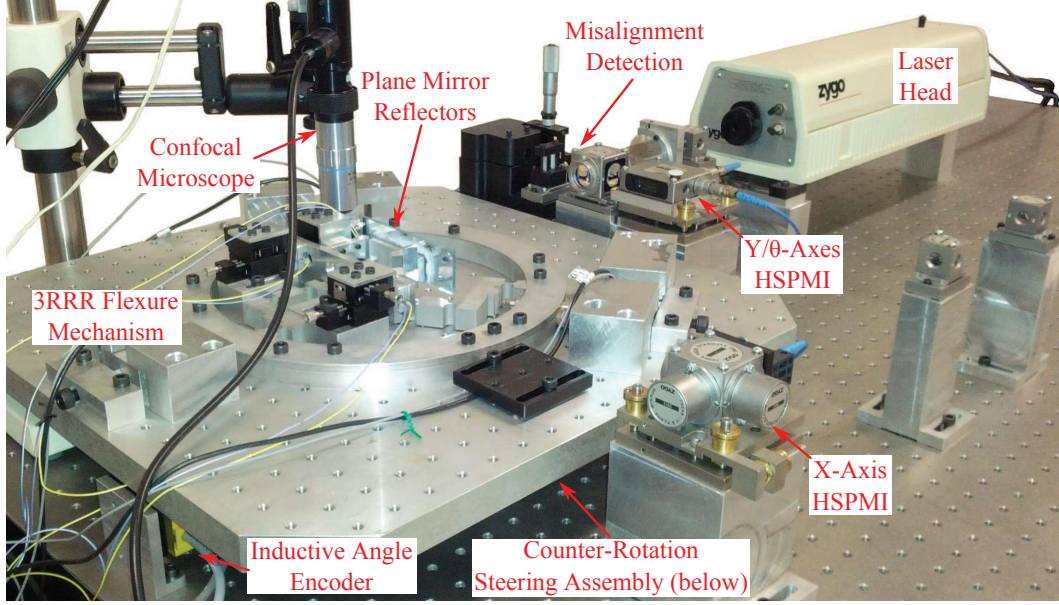
Figure 4: Photograph of experimental apparatus.

is capable of 50,800 steps per revolution, and its coupling to the stage provides a further 45 times gear reduction. Hence, a rotational resolution of 2.74 μrad is achievable in a single step. Attached to the shaft of the motor is an inductive angle encoder capable of 65,536 counts per revolution – thus angular displacement of the stage is measurable with a resolution of 2.13 μrad. Measurement of the rotation of the mechanism's base is performed directly with a vision-based technique utilizing a confocal microscope and micrometer scale calibration slide. Details of this technique have been covered in prior research [41]. Utilizing this technique, the angular displacement can be measured with 0.29 μrad resolution over a 7.46 mrad range, limited only by the length of the calibration slide.

Misalignment of the measurement beams is detected by a PSD-based detection unit, which will be described in Section 3.1. Two High-Stability Plane Mirror Interferometers (HSPMI) are mounted along the X and Y axes (when the mechanism is in its unactuated state). The X axis HSPMI records only linear motion. The HSPMI unit in the Y direction also provides a redundant yaw axis, which is instead measured by the misalignment detection system. A photograph of the experimental apparatus is shown in Fig. 4.

A computer using a real-time extension performs the data acquisition and analysis, control computations, and actuation tasks. This control computer utilizes 16-bit digital-to-analogue and analogue-to-digital converters. Control tasks are performed at 125 Hz, whilst commands to the actuator for the steering assembly can be issued at up to 25 kHz, permitting a maximum angular velocity of 68 mrad/s.
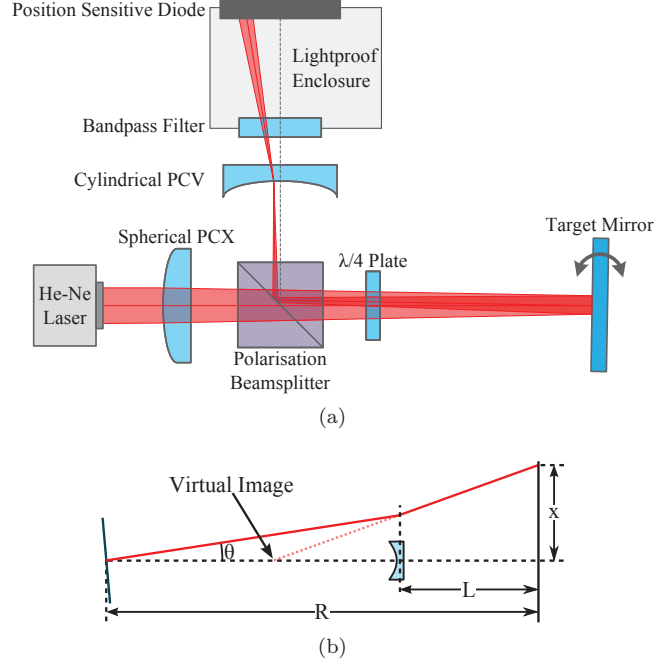
5

Figure 5: Schematic diagram of the PSD-based misalignment detection methodology: (a) Arrangement of components, (b) Ray tracing diagram for determination of amplification factor.

3.1 Misalignment Detection Methodology

A novel measurement methodology to measure the misalignment of the laser beam has been developed using a PSD. The approach differs from those of Pisani and Astrua [31] and Zheng *et al.* [32] through the use of a concave lens to amplify the measured displacement. Fig. 5a shows a schematic of the proposed measurement technique.

Without the concave-convex lens pair, the deviation of the laser beam, x, measured a distance R from the target mirror (through the beamsplitter) by the PSD would be approximately the arc length:

$$x = R \tan \theta \approx R\theta \tag{1}$$

The only parameter which can be adjusted to increase the resolution is the distance to the sensor. Therefore, large distances are required to achieve adequate resolution. Amplification of this deflection is increased through the addition of a cylindrical plano-concave (PCV) lens placed before the PSD. If the PCV lens with focal length f is placed at a distance L before the PSD, the thin lens formula, together with the ray tracing diagram shown in Fig. 5b allows the determination of the displacement of the laser beam by (2).

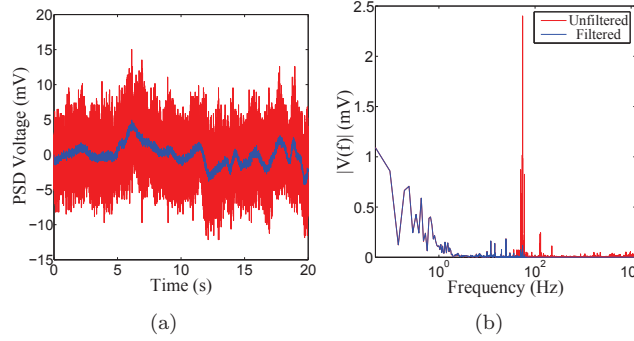$$x = \frac{R|f| + L(R - L)}{|f|} \tan \theta \tag{2}$$

Figure 6: Noise within voltage output of misalignment detection sensor: (a) time domain, (b) frequency domain.

The resolution can be increased not only through increasing R, but also by decreasing the focal length and changing the distance of the lens from the sensor. However, the introduction of the PCV lens has an unwanted consequence of causing the beam spot to diverge, which can cause the beam reaching the PSD to be larger than its active area, or at least reduce the photocurrent, and thus increasing noise. These effects are mitigated by the placement of a plano-convex (PCX) lens before the beamsplitter, focusing the beam at approximately the position of the PCV lens. The beam does not diverge significantly between the PCV lens and the sensor, and thus a small elliptical beam spot is incident on the PSD.

Instead of a standard beamsplitter, a polarization beamsplitter and quarter waveplate are used to allow the misalignment detection PSD to share the heterodyne laser source used for the two HSPMIs. The PSD is housed within a lightproof enclosure to reduce noise from stray radiation such as heat and ambient room lighting. The entrance into the enclosure utilizes a bandpass filter to prevent light other than that at the laser frequency from reaching the sensor.

The voltage output of the PSD system with a stationary reflector can be seen in Fig. 6. The dominant source of noise within the raw signal was observed at 50 Hz due to the ambient room lighting and other electrical interference. An 8th order digital Butterworth filter with a corner frequency of 30 Hz has been applied to the data, which produces significant improvement in the output. After filtering, the noise in the output was less than 5 mV.

The stage was rotated through the full measurement range of the PSD, limited by the 12 mm length of the sensor. Fig. 7 shows the output against the yaw reading of the HSPMI. Within about 500 μrad of the zero position, the output voltage of the PSD and the angular displacement were seen to be directly proportional to each other, as expected from (2). This occurred whilst the beamspot fell entirely on the active region of the PSD. Outside of this region, the PSD's output saturated, producing the non-linear output curve seen in the figure. From Fig. 7, it can be observed that conversion from the voltage to the angular displacement can be performed using the constant of proportionality, found to be 101.4 μrad/V. The resolution will be limited by the noise of the signal, and is therefore 0.5 μrad.
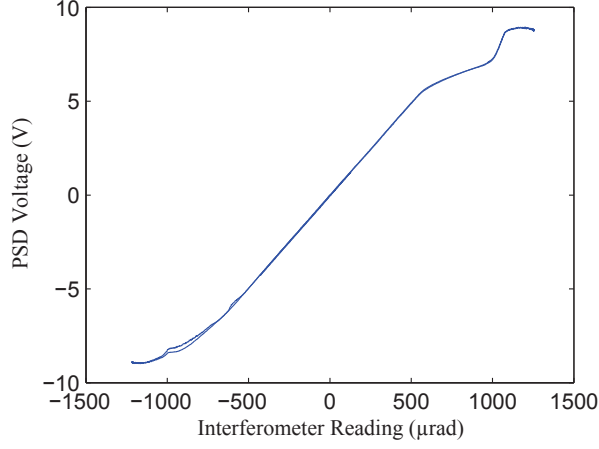
7

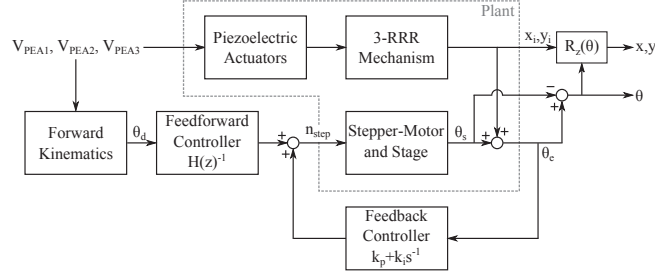Figure 7: Measurement of angular misalignment using PSD-based methodology.

Figure 8: Proposed control methodology for misalignment compensation.

4 Controller Methodology

It is proposed that a compound feedforward-feedback controller be utilized to drive the steering assembly providing the counter-rotation. The feedforward component, which is an inversion of a model of the stepper-stage dynamics $(H(z)^{-1})$, provides the coarse input to the motor, whilst the feedback component acts to eliminate the misalignment of the measurement beams of the interferometry-based measurement system. The θ_d input into the feedforward component is provided by the forward kinematics of the flexure-based mechanism. A schematic of this control methodology is shown in Fig. 8.

A PI controller can be utilized for the feedback component of the control methodology. The error input to this controller is the misalignment measured by the PSD, representing the discrepancy between the rotation of the 3-RRR stage and the counter-rotation of the steering assembly.

As shown in Fig. 8 the θ displacement is given by the difference between the PSD misalignment measurement θ_e and the counter-rotation θ_s (provided by the vision-based measurement), as given by:

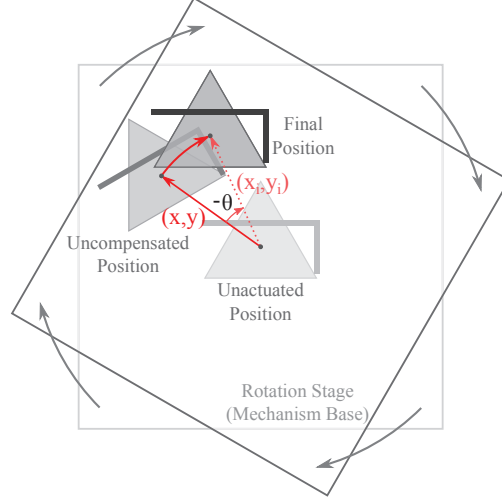$$\theta = \theta_e - \theta_s \tag{3}$$

8

Figure 9: Coordinate transformation resulting from counter-rotational motion.

The linear position of the 3-RRR stage can be determined by combining the information obtained from the two linear interferometer axes with the measurement of the angular position. Fig. 9 shows a schematic diagram of the mechanism positioning in response to a coupled motion. Due to the rotation of the stage, which is centered at the location of the end-effector in the unactuated position, the (x_i, y_i) coordinates measured by the linear interferometer axes will not measure X and Y directly. As shown in Fig. 9, the desired coordinates (x, y) are rotated by an angle $-\theta$ in the frame of the interferometers due to the counter-rotation. Hence, a rotation by θ is required to transform these measurements into the frame of the mechanism's base. This can be performed using a simple 2×2 transformation matrix R_z via (4).

$$\begin{bmatrix} x \\ y \end{bmatrix} = R_z(\theta) \begin{bmatrix} x_i \\ y_i \end{bmatrix} = \begin{bmatrix} \cos\theta & -\sin\theta \\ \sin\theta & \cos\theta \end{bmatrix} \begin{bmatrix} x_i \\ y_i \end{bmatrix} \tag{4}$$

4.1 System Identification and Control Performance Optimisation

A model of the system has been produced which has been inverted for the proposed feedforward control methodology. A sinusoidal signal with the frequency exponentially varying from 0.05 Hz to 20 Hz has been used as the control input to the stepper motor, in order to excite the modes of vibration of the stage. The amplitude of the oscillation is 150 μrad to allow the misalignment sensor to be used to measure the response. The PEA inputs were kept at a preload of 25 V throughout the experimental operation. Fig. 10 shows the frequency response of the stepper motor during this excitation.

It can be seen that a resonance peak is encountered at about 16 Hz. A discrete-time linear system model has been identified from the frequency response. Fig. 10 also shows the response for the identified system. The discrete-time transfer function (at a sampling rate of 125 Hz) is as follows:
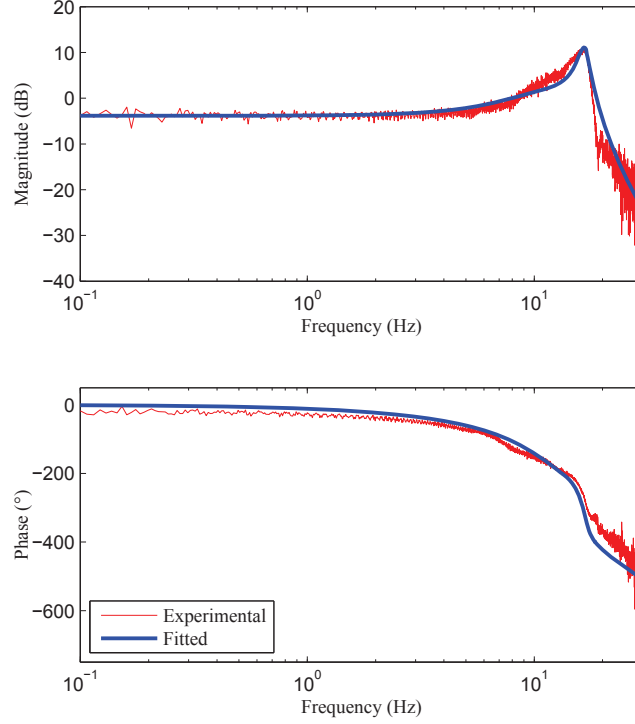
Figure 10: Frequency response of stepper-motor rotation stage.

$$H(z) = \frac{\theta_s}{\theta_d}(z)$$
$$= \frac{0.0967}{z^4 - 2.619z^3 + 3.203z^2 - 1.959z + 0.5254} \tag{5}$$

Tuning of the PI controller has been investigated utilizing the common Ziegler-Nichols method. However, it has been found that the proportional gain which causes the plant to become unstable is inversely related to the magnitude of the initial misalignment error. In other words, the steering assembly's response is non-linear. Utilizing a small gain ensures the system remains stable at the cost of slow response. Conversely, due to the steering assembly having a minimum step size, setting a higher gain allows small errors to continually be corrected, but would cause instability in the event of any significant disturbances. To account for these considerations, it is proposed that a varying proportional gain dependent upon the magnitude of the error be utilized, as given in (6).

$$k_p = A \exp(-k|\theta_e|) + B \tag{6}$$

where A, B, and k are adjustable positive parameters. B is chosen to be the largest gain for which the response is stable for all errors. For large errors, the decaying exponential term would be approximately zero, and thus the proportional gain is approximately B. For small errors of the magnitude of a single
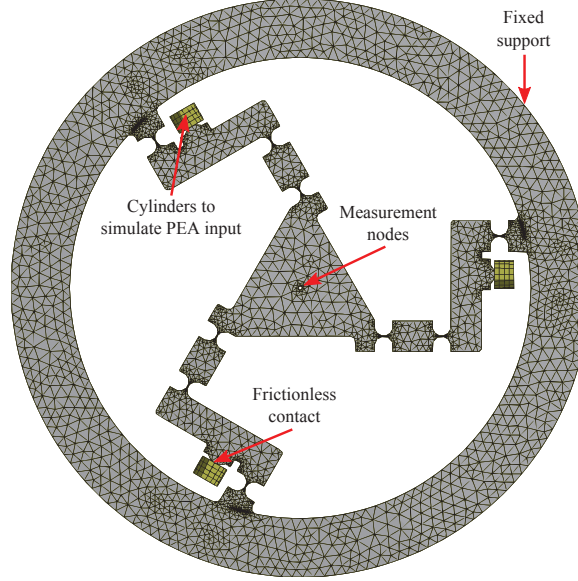
Figure 11: Finite element model of 3-RRR mechanism for computational workspace analysis.

step, the exponential term is approximately one, hence the gain is approximately $A + B$. A is therefore chosen to allow the system to be responsive to small errors. The decay constant k is chosen to provide a suitable transition between these regimes.

5   Workspace Identification of 3-RRR Mechanism

Experimentation to determine the workspace of the mechanism has been performed as a means to verify the ability of the proposed counter-rotation methodology to extend the angular range whilst enabling pose measurement. From an initial preload of 25 V on each PEA, the mechanism was driven between each of the eight combinations of actuating each PEA with either 0 V or 100 V. This operation allowed the edges of the workspace boundary to be identified. Command voltages were changed linearly, with transitions between each motion smoothed by quadratic sections.

For comparison, Finite Element Modeling (FEM) of the 3-RRR stage has been performed. A meshed model of the mechanism is shown in Fig. 11. Cylinders along the axis of each actuator have been used to provide the input displacement to the mechanism. Standard ten-node tetrahedral elements have been utilized for the model, and frictionless contact elements provide the connection at the actuation points to the input cylinders. The magnitude of the displacement inputs is calculated from experimental data, using the mean of the stiffnesses of the PEAs (in μm/V) as measured by strain gauges mounted on each actuator. A static structural analysis using ANSYS has been employed to perform the computational analysis.

The misalignment of the laser beam measured by the PSD during experimentation is shown in Fig. 12. The misalignment was observed to have an RMS value of 2.7 μrad, which is the error of the controller
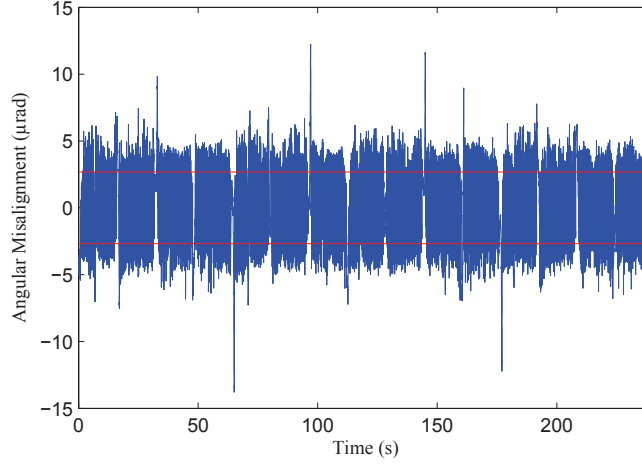
11

Figure 12: Misalignment measured by PSD during traversal of workspace boundary. The horizontal red lines indicate the RMS misalignment.
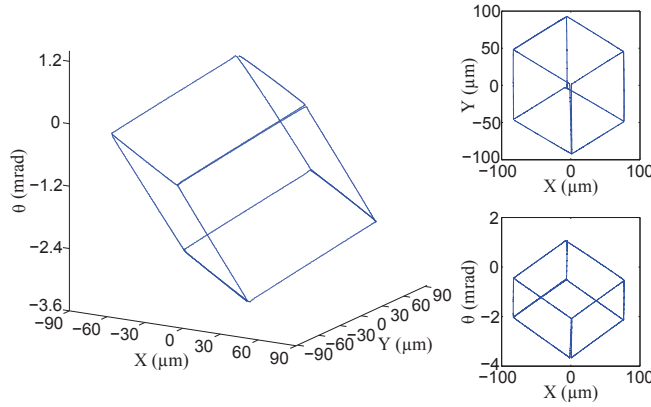
Figure 13: Workspace of 3-RRR mechanism as measured using the misalignment compensation methodology.

coupled with the noise from the PSD output. This value is less than the step resolution of the stepper motor. The RMS measurement error is therefore 3 μrad, due to the misalignment and vision-based system errors.

The workspace boundary established during experimentation is shown in Fig. 13. Table 1 compares the workspace established by experimentation using the counter-rotation methodology with the output of the computational analysis.

6 Discussion

The results of the previous section demonstrate the ability of the proposed misalignment compensation methodology to enable pose measurement of three DOF planar motions over a large range.

12

Table 1: Comparison of experimental and computational workspace extrema

		Minimum	Maximum	Range
x	Experimental	-83.22 ± 0.06 μm	77.25 ± 0.05 μm	160.47 ± 0.08 μm
	FEA	-79.6 μm	79.6 μm	159.3 μm
y	Experimental	-92.40 ± 0.07 μm	92.59 ± 0.05 μm	184.99 ± 0.08 μm
	FEA	-92.0 μm	91.9 μm	183.9 μm
θ	Experimental	-3.675 ± 0.003 mrad	1.058 ± 0.003 mrad	4.733 ± 0.004 mrad
	FEA	-4.091 mrad	1.364 mrad	5.455 mrad

Experimental results compare favorably to those found through computational analysis. Discrepancies between these two sets of results are mainly due to the hysteresis of the PEAs. Furthermore, using the mean PEA stiffness to calculate the actuation limits simplifies the analysis, when in reality each PEA exhibits a slightly different response and maximum displacement.

The errors in θ measurement result from any uncompensated misalignment, in addition to the maximum resolution of the vision-based measurement technique. However, the errors in the linear axes will have sources in both the counter-rotation provided by the steering assembly as well as those inherent to the laser-interferometry-based measurement method. The largest of these will be due to the center of the unactuated mechanism's end effector being displaced from the axis of rotation of the stage. As the stage rotates, this position will move along a circular arc (in the X-Y plane) about the axis of rotation, which will be coupled to the desired X-Y motion. For the stage utilized, this displacement is less than 25 μm. In the worst case, for the maximum -3.675 mrad displacement, this added error will be approximately 91.9 nm. The RMS steady-state error of the linear interferometer axes was found to be 44.1 nm. Therefore, at the maximum rotation the total error in each axis is found to be 101.9 nm. These errors can be reduced through the use of a more precise rotation stage, and the use of shielding to prevent environmental conditions affecting the optical setup.

In coupling the positioning mechanism to the steering mechanism, the two rotation axes will not be perfectly parallel. By considering the deviation of the measurement beam due to a vertical misalignment by an angle β, where the distance from the target reflector to the HSPMI is R_i, the measurement error can be found as (7).

$$\Delta x = \frac{1}{2} R_i \left(1 - \cos \theta_e\right) \left(\cos 2\beta + 1\right) \tag{7}$$

This is a cosine error coupled with the effects of the axis misalignment. As this error will vary as θ_e^2, which will be minimized using the proposed methodology, this error will be negligible.

As shown in Fig. 4, an encoder was mounted directly onto the drive shaft of the stepper-motor before the 45-times gear reduction. Despite the rotation stage being preloaded to remove backlash, hysteresis was observed between the encoder reading and the rotation of the reflector. The use of a method to measure the stage rotation directly, provided by the vision-based measurement technique in this case, is necessary in order to gain an accurate measurement of the stage rotation. However, as opposed to

13

the use of the encoder, the frame rate of the camera ultimately places limits on the maximum speed of rotation and the feedback rate for control tasks with the micro/nano positioning stage.

The system model of the stepper-stage, (5), which was inverted for use in the feedforward component of the control methodology was linear. However, the difficulties in tuning which led to the development of the feedback controller provided by (6) demonstrate that the steering assembly's dynamics are non-linear. It is therefore expected that the identification of a linear model would be dependent on the amplitude of the excitation utilized. For the trajectory used to examine the mechanism's workspace, it was found that the feedforward controller alone (with feedback gains set to zero) would yield a maximum misalignment error of about 100 μrad. However, by adding a gain to the feedforward controller (kH^{-1}), it was found through manual tuning that the error was minimized with unity gain. Hence, this system inversion utilized is likely to be the most accurate when restricted to linear models. To improve the accuracy of the feedforward controller, more advanced system identification techniques would be required.

Despite these observations, the RMS misalignment error was kept below the step resolution of the actuation system by the compound feedforward-feedback controller. As the feedback controller was able to decrease the misalignment to this level, the use of a linear model of the steering assembly was satisfactory. Further reductions in the misalignment error and rotational precision can therefore be made through improvements in the source of rotational motion. This could potentially be achieved through the use of a direct drive motor to overcome the limitations of fixed stepping distance and discontinuous stepping motion. Furthermore, Fig. 10 indicates the system bandwidth is 18 Hz, which is likely to reduce for larger amplitude oscillations. This bandwidth could be improved by reducing the rotational inertia of the mechanism base.

7   Conclusion

This paper has presented a methodology through which the pose of a micro/nano positioning stage can be measured over a large range in both linear and angular axes of motion. A novel PSD-based misalignment sensing technique has been developed which can measure small angular displacements with high resolution. A feedforward-feedback compound control methodology has been proposed to eliminate misalignment errors, and hence improve measurement outputs. Experimental results have demonstrated the potential of the methodology to extend the angular measurement range whilst permitting the simultaneous use of linear-interferometry-based sensing techniques for linear axis measurement. Furthermore, these results have shown the capability of the methodology to minimize misalignment errors down to the resolution of the source of rotation of the steering assembly.

References

[1] G. Binnig and D. P. E. Smith, "Single-tube three-dimensional scanner for scanning tunneling microscopy," *Review of Scientific Instruments*, vol. 57, no. 8, p. 1688, 1986.

[2] Y. Tian, D. Zhang, and B. Shirinzadeh, "Dynamic modelling of a flexure-based mechanism for ultra-precision grinding operation," *Precision Engineering*, vol. 35, no. 4, pp. 554–565, 2011.

[3] K.-B. Choi and J. J. Lee, "Passive compliant wafer stage for single-step nano-imprint lithography," *Review of Scientific Instruments*, vol. 76, no. 7, p. 075106, 2005.

[4] D. Kim, D. Kang, J. Shim, I. Song, and D. Gweon, "Optimal design of a flexure hinge-based XYZ atomic force microscopy scanner for minimizing Abbe errors," *Review of Scientific Instruments*, vol. 76, no. 7, p. 073706, 2005.

[5] M. N. Mohd Zubir and B. Shirinzadeh, "Development of a high precision flexure-based microgripper," *Precision Engineering*, vol. 33, no. 4, pp. 362–370, 2009.

[6] B. J. Kenton and K. K. Leang, "Design and control of a three-axis serial-kinematic high-bandwidth nanopositioner," *IEEE/ASME Trans. Mechatronics*, vol. 17, no. 2, pp. 356–369, 2012.

[7] G. A. Al-Kindi and B. Shirinzadeh, "An evaluation of surface roughness parameters measurement using vision-based data," *International Journal of Machine Tools and Manufacture*, vol. 47, no. 3-4, pp. 697–708, 2007.

[8] H. Adriaens, W. De Koning, and R. Banning, "Modeling piezoelectric actuators," *IEEE/ASME Trans. Mechatronics*, vol. 5, no. 4, pp. 331–341, 2000.

[9] L.-J. Lai, G.-Y. Gu, and L.-M. Zhu, "Design and control of a decoupled two degree of freedom translational parallel micro-positioning stage." *Review of Scientific Instruments*, vol. 83, no. 4, p. 045105, 2012.

[10] Y. Li and Q. Xu, "Design and robust repetitive control of a new parallel-kinematic XY piezostage for micro/nanomanipulation," *IEEE/ASME Trans. Mechatronics*, vol. 17, no. 6, pp. 1120–1132, 2012.

[11] S. Polit and J. Dong, "Development of a high-bandwidth XY nanopositioning stage for high-rate micro-/nanomanufacturing," *IEEE/ASME Trans. Mechatronics*, vol. 16, no. 4, pp. 724–733, 2011.

[12] Y. K. Yong, S. S. Aphale, and S. O. R. Moheimani, "Design, identification, and control of a flexure-based XY stage for fast nanoscale positioning," *IEEE Trans. Nanotechnol.*, vol. 8, no. 1, pp. 46–54, 2009.

[13] J.-P. Bacher, S. Bottinelli, J.-M. Breguet, and R. Clavel, "Delta3 : design and control of a flexure hinges mechanism," in *Proc. SPIE 4568, Microrobotics and Microassembly III*, vol. 4568, 2001, pp. 135–142.

[14] Y. Tian, B. Shirinzadeh, D. Zhang, and G. Alici, "Development and dynamic modelling of a flexure-based ScottRussell mechanism for nano-manipulation," *Mechanical Systems and Signal Processing*, vol. 23, no. 3, pp. 957–978, 2009.

[15] L. Chassagne, M. Wakim, S. Xu, S. Topçu, P. Ruaux, P. Juncar, and Y. Alayli, "A 2D nano-positioning system with sub-nanometric repeatability over the millimetre displacement range," *Measurement Science and Technology*, vol. 18, no. 11, pp. 3267–3272, 2007.

[16] H. C. Liaw and B. Shirinzadeh, "Neural Network Motion Tracking Control of Piezo-Actuated Flexure-Based Mechanisms for Micro-/Nanomanipulation," *IEEE/ASME Trans. Mechatronics*, vol. 14, no. 5, pp. 517–527, 2009.

[17] Y. Cao, L. Cheng, X. B. Chen, and J. Y. Peng, "An inversion-based model predictive control with an integral-of-error state variable for piezoelectric actuators," *IEEE/ASME Trans. Mechatronics*, vol. 18, no. 3, pp. 895–904, 2013.

[18] H. C. Liaw and B. Shirinzadeh, "Robust adaptive constrained motion tracking control of piezo-actuated flexure-based mechanisms for micro/nano manipulation," *IEEE Trans. Ind. Electron.*, vol. 58, no. 4, pp. 1406–1415, 2011.

[19] Y. Qin, B. Shirinzadeh, Y. Tian, and D. Zhang, "Design issues in a decoupled XY stage: Static and dynamics modeling, hysteresis compensation, and tracking control," *Sensors and Actuators A: Physical*, vol. 194, pp. 95–105, 2013.

[20] M. A. Janaideh and P. Krejčí, "Inverse rate-dependent Prandtl Ishlinskii model for feedforward compensation of hysteresis in a piezomicropositioning actuator," *IEEE/ASME Trans. Mechatronics*, vol. 18, no. 5, pp. 1498–1507, 2013.

[21] Y. Xie, Y. Tan, and R. Dong, "Nonlinear modeling and decoupling control of XY micropositioning stages With piezoelectric actuators," *IEEE/ASME Trans. Mechatronics*, vol. 18, no. 3, pp. 821–832, 2013.

[22] Y. Qin, Y. Tian, D. Zhang, B. Shirinzadeh, and S. Fatikow, "A novel direct inverse modeling approach for hysteresis compensation of piezoelectric actuator in feedforward applications," *IEEE/ASME Trans. Mechatronics*, vol. 18, no. 3, pp. 981–989, 2013.

[23] H. Wang and X. Zhang, "Input coupling analysis and optimal design of a 3-DOF compliant micro-positioning stage," *Mechanism and Machine Theory*, vol. 43, no. 4, pp. 400–410, 2008.

[24] L. L. Cheng, J. W. Yu, and X. F. Yu, "Design and analysis of a 6-DOF monolithic nanopositioning stage," *Key Engineering Materials*, vol. 437, pp. 61–65, 2010.

[25] B.-j. Yi, G. B. Chung, H. Y. Na, W. K. Kim, and I. H. Suh, "Design and experiment of a 3-DOF parallel micromechanism utilizing flexure hinges," *IEEE J. Robot. Autom.*, vol. 19, no. 4, pp. 604–612, 2003.

[26] Y. Tian, B. Shirinzadeh, and D. Zhang, "Design and dynamics of a 3-DOF flexure-based parallel mechanism for micro/nano manipulation," *Microelectronic Engineering*, vol. 87, no. 2, pp. 230–241, 2010.

[27] Y. K. Yong and T.-F. Lu, "Kinetostatic modeling of 3-RRR compliant micro-motion stages with flexure hinges," *Mechanism and Machine Theory*, vol. 44, no. 6, pp. 1156–1175, 2009.

[28] J. Yuan and X. Long, "CCD-area-based autocollimator for precision small-angle measurement," *Review of Scientific Instruments*, vol. 74, no. 3, p. 1362, 2003.

[29] Q. Liu, Y. Li, W. Zhao, and X. Hu, "Two dimensions angular sensor for micro/nano measurement," in *IEEE International Conference on Nano/Micro Engineered and Molecular Systems*, Bangkok, Thailand, 2007, pp. 274–277.

[30] T. Suzuki, T. Endo, O. Sasaki, and J. E. Greivenkamp, "Two-dimensional small-rotation-angle measurement using an imaging method," *Optical Engineering*, vol. 45, no. 4, p. 043604, 2006.

[31] M. Pisani and M. Astrua, "Angle amplification for nanoradian measurements." *Applied optics*, vol. 45, no. 8, pp. 1725–9, 2006.

[32] D. Zheng, X. Wang, and O. Sasaki, "Parallel plate interferometer with a reflecting mirror for measuring angular displacement," *Optical Review*, vol. 14, no. 5, pp. 314–318, 2007.

[33] Z. Ge and M. Takeda, "High-resolution two-dimensional angle measurement technique based on fringe analysis." *Applied optics*, vol. 42, no. 34, pp. 6859–68, 2003.

[34] J.-h. Zhang and C.-H. Menq, "A linear/angular interferometer capable of measuring large angular motion," *Measurement Science and Technology*, vol. 10, no. 12, pp. 1247–1253, 1999.

[35] H.-C. Yeh, W.-T. Ni, and S.-S. Pan, "Real-time motion control With subnanometer heterodyne interferometry," *International Journal of Modern Physics D*, vol. 11, no. 07, pp. 1087–1099, 2002.

[36] Y.-M. Choi, J. J. Kim, J. Kim, and D.-G. Gweon, "Design and control of a nanoprecision XYΘ scanner." *Review of Scientific Instruments*, vol. 79, no. 4, p. 045109, 2008.

[37] J. Hrabina, J. Lazar, P. Klapetek, and O. Číp, "Multidimensional interferometric tool for the local probe microscopy nanometrology," *Measurement Science and Technology*, vol. 22, no. 9, p. 094030, 2011.

[38] J. Lazar, P. Klapetek, O. Číp, M. Čížek, and M. Šerý, "Local probe microscopy with interferometric monitoring of the stage nanopositioning," *Measurement Science and Technology*, vol. 20, no. 8, p. 084007, 2009.

[39] U. Bhagat, B. Shirinzadeh, Y. Tian, and D. Zhang, "Experimental analysis of laser interferometry-based robust motion tracking control of a flexure-based mechanism," *IEEE Trans. Autom. Sci. Eng.*, vol. 10, no. 2, pp. 267–275, 2013.

[40] B. Shirinzadeh, P. L. Teoh, Y. Tian, M. Dalvand, Y. Zhong, and H. C. Liaw, "Laser interferometry-based guidance methodology for high precision positioning of mechanisms and robots," *Robotics and Computer-Integrated Manufacturing*, vol. 26, no. 1, pp. 74–82, 2010.

[41] L. Clark, B. Shirinzadeh, U. Bhagat, and J. Smith, "A vision-based measurement algorithm for micro/nano manipulation," in *2013 IEEE/ASME International Conference on Advanced Intelligent Mechatronics*. Wollongong, Australia: IEEE, 2013, pp. 100–105.